Journal of Thermal Analysis and Calorimetry, Vol. 57 (1999) 607-622

KINETICS OF SOLUTE FLOW TO PARTIAL DISLOCATION IN Cu–3.4 AT.% Sb

A. Varschavsky and E. Donoso

Universidad de Chile, Facultad de Ciencias Físicas y Matemáticas, Instituto de Investigaciones y Ensayes de Materiales, IDIEM Casilla 1420, Santiago, Chile

(Received December 22, 1998)

Abstract

The kinetics of solute segregation to partial dislocations in a Cu–3.4 at.% Sb alloy was studied by using a phenomenological approach with differential scanning calorimetry and isothermal calorimetry. The material, severely deformed by repeated bending, presented an excess of dissociated edge dislocations with a dislocation density amounting to about $8.5 \cdot 10^{14}$ m^{-2}, calculated using a prior model of the authors, together with calorimetric recrystallization trace analysis. The kinetics was found to be ruled by two overlapping mechanisms: diffusion of solute atoms mostly through dislocation pipes in the initial and middle stages of the reaction process, acting together with bulk solute diffusion in these stages and later. Bulk solute diffusion increases as the reaction proceeds, as shown by the increasing values of apparent activation energy in the reaction. The exponent of the Mehl-Johnson-Avrami equation used in the phenomenological description was successfully fitted to a time–temperature-dependent function, increasing in agreement with the apparent activation energy behaviour, as may be expected.

Keywords: Cu–3.4 at.% Sb alloy, kinetics

Introduction

In solid solutions of deformed Cu annealed below the recrystallization temperature, a hardening effect [1–4] called anneal hardening [5–11] is produced through the interaction of solute atoms with lattice defects. This effect may cause a considerable increase in flow stress, in which solute locking to dislocations plays the most important role [12, 13], although solute segregation to stacking faults may not be disregarded [14]. The above phenomenon is important as concerns not only elucidation of the hardening mechanism, but also investigations of static and dynamic strain ageing [15–18] and strain sensitivity determinations. We have modelled solute-dislocation pinning effects in previous papers [3, 4, 19], quantitatively testing the hypothesis that this is the main cause of the predominant hardening mechanism. The model, based on energetic considerations, is very suitable together with differential scanning calorimetry (DSC) for assessing dislocation densities and energy balances compatible with the segregation process. The kinetics of solute anchoring to partial dislocations in deformed Cu solid solutions is important; recent research [20, 21] led

1418–2874/99/ $ 5.00

Akadémiai Kiadó, Budapest
Kluwer Academic Publishers, Dordrecht

to a model based on a previous one for predicting the kinetics of the pinning process, and tested its validity in cold-rolled Cu–19 at.% Al and Cu–5 at.% Mn, using isothermal microcalorimetry. That research revealed that the model predicted two hitherto unknown processes in the kinetics of solute segregation to partial dislocations during isothermal experiments, and that these processes actually occur in both alloys [20, 21]. The research also confirmed that half-edge and half-screw dislocations are present under this deformation mode and that, most importantly, segregation rates increase with dislocation density and are larger for screw than for edge dislocations. Another important feature was that most segregation takes place by pipe diffusion along the partials. However, the model was unable to predict and confirm experimentally that the overall activation energy of the segregation process may change during the kinetic path as envisaged [20, 21], mainly due to the lack of resolution introduced by the above processes, which overlap to some extent, and to the characteristics of the alloys studied. It is to be expected that the two types of diffusion mechanisms involved, namely bulk and pipe diffusion along the partials [20, 21], should produce variations in activation energy during the segregation reaction and also in the exponent of the Mehl-Johnson-Avrami (MJA) equation governing each process. For the present study, we chose a Cu–3.4 at.% Sb alloy for the following reasons:

a) Cu–Sb diluted alloys exhibit one of the highest stacking fault probabilities among Cu alloys [22], so that almost all dislocations slip out in partials.

b) Cu–Sb alloys have the largest reported solute-dislocation binding energy [4], as expected from the extremely large atomic misfit value.

On the other hand, to suppress one of the above-mentioned segregation processes (segregation to edge components of dissociated screw dislocations that exhibit lower binding energies), a large plastic deformation introduced by repeated bending was chosen in the present study, since mostly dissociated edge dislocations are expected to develop, as will be seen later.

Formal treatment of segregation kinetics

In section dealing with dislocation character distribution, it will be stated that the energy ΔH_d evolved during the segregation of solute atoms to partial dislocations corresponding to a dissociated edge can be described by Eq. (11) (presented below). During segregation, the evolved heat $\Delta H(t)$ at time t is a function of the kinetic path of solute concentration $c_e(t)$ before equilibrium value c_{de} is reached

$$\Delta H(t) = 2\pi \frac{\rho}{c} b^2 \Delta H_{ae} c_e(t) \tag{1}$$

The effective solute composition at arrested dislocations is determined by the ageing time. Sundry models based on diffusion and drift of the solute in the stress fields of dislocations have been designed to explain the various time dependences found. General Cottrell-Bilby solute concentration kinetics is assumed as a starting point [23]

$$c_e(t) = c(K_e Dt)^{n_b} \tag{2}$$

where D is the effective solute diffusion coefficient of the underlying process, while K_e is a constant depending on the solute-dislocation binding energy. In the original Cottrell-Bilby model, n_b=2/3. This expression is valid only for the early stages of segregation. If a Louat correction [24] of the general Cottrell-Bilby analysis used here to include saturation at longer ageing times is applied when the maximum number of pinners that may be accommodated in the dislocation core is considered, then Eq. (2) become

$$c_e(t) = c_{de}\left[1 - \exp\left(-\frac{c(K_e Dt)^{n_b}}{c_{de}}\right)\right] \tag{3}$$

where c_{de} is the equilibrium segregated solute concentration. With the above assumptions and considering $D=D_o\exp(-Q_b/RT)$, where D_o is the diffusion constant and Q_b is the activation energy for bulk solute diffusion, Eqs (3) and (1) yield

$$\Delta H(t) = 2\pi \frac{\rho}{c} b^2 \Delta H_{ae} c_{de}[1 - \exp[-K_f t^{n_b}]] \tag{4}$$

where

$$K_f = K_o \exp\left[-\frac{Q_f}{RT}\right] \tag{5}$$

Here $Q_f=(n_b Q_b - \Delta H_{ae})$ is the apparent activation energy for the overall process, and $K_o=(K_e D_o)^n$. If the reacted fraction associated with segregation is

$$y = \frac{\Delta H(t)}{\Delta H_d} \tag{6}$$

then Eqs (4) and (11) yield

$$y = 1 - \exp(-K_f t^{n_b}) \tag{7}$$

on the basis of this treatment.

Materials and experimental procedure

The alloy employed was prepared in a Baltzer VSG 10 vacuum furnace by using electrolytic Cu (99.95% purity) and Sb (99.9% purity). Chemical analysis showed that this alloy contained 3.4 at.% Sb. The ingot was hot-forged at 1123 K to a thickness of 20 mm, pickled with nitric acid solution (15%) in distilled water to remove surface oxide, annealed at 1123 K for 72 h to achieve homogeneity, and cooled in the furnace to room temperature. The ingot was then cold-rolled to 2.0 mm thickness, with intermediate anneals at 1123 K for 1 h. After the last anneal, the material was

cold-rolled to 1.0 mm thickness (50% reduction) and recrystallized at 680 K for 1 h. Repeated plastic bending was performed around a mandrel 60 mm in diameter, until a microhardness of about 281 HV was reached, which is comparable to the 293 HV obtained after 50% cold-rolling, corresponding to dislocation densities of about 10^{15} m^{-2} .

Microcalorimetric analysis of the samples was performed in a DuPont 2000 thermal analyser. Specimen discs 1.0 mm thick and 6 mm in diameter were prepared for each material condition. DSC measurements of heat flow were made in the constant-heating mode (heating rate 0.083 K s^{-1}). Tests were carried out from room temperature up to 860 K. To increase the sensitivity of measurements, in each case a high-purity, well-annealed Cu disc was used as a reference, the mass of which was approximately equal to that of the sample, and in which no thermal events occurred over the range of temperatures scanned. In order to minimize oxidation, dried nitrogen was passed through the calorimeter ($0.8 \cdot 10^{-4}$ m^3 min^{-1}). After each test, the data were converted to a differential heat capacity *vs.* temperature form, using a previously established calibration for the DSC cell. Subsequently, a linear baseline was subtracted from the data. This baseline represents the temperature-dependent heat capacity of the Cu–Sb solid solution under the existing thermal conditions; its value was in agreement with the Kopp-Neumann rule.

The heat capacity remainder, namely the differential heat capacity ΔC_p, represents the heat associated with the solid-state reactions during the DSC run. Thus, the reaction peaks in the ΔC_p *vs.* T curves can be characterized by a reaction enthalpy of a particular event.

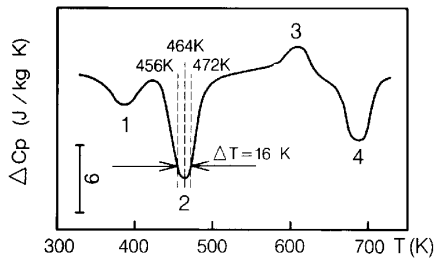

Fig. 1 DSC trace for Cu–3.34 at.% Sn severely deformed in pull-release bending. The temperatures chosen to perform isothermal calorimetric runs associated with solute segregation to partial dislocations are indicated. This trace is the average of 5 runs. (Heating rate: 0.083 K s^{-1})

Isothermal calorimetry was performed at three temperatures (456, 464 and 472 K) in the narrow temperature half-width range ΔT=16 K of the stage corresponding to the segregation process, as shown in the thermoanalytical curve in Fig. 1.

Results

DSC curves

A typical thermoanalytical curve at the indicated heating rate is shown in Fig. 1: differential heat capacity ΔC_p *vs.* temperature curves for the deformed material char-

acterized by three exothermic reactions, stages 1, 2 and 4, and an endothermic reaction, designated stage 3.

The four stages observed are connected with the following processes, by analogy with Cu–3.34 at.% Sn, because of the similarities between the two alloys and also because of their identical DSC trace features [4]:

Stage 1: Incomplete formation of δ′ phase nucleated at dislocations (ε′ in the case of Cu–3.34 at.% Sn [4]).

Stage 2: Solute segregation to partial dislocations, the topic of the present study.

Stage 3: Dissolution of δ′.

Stage 4: Recrystallization.

In order to estimate dislocation densities as a necessary input for evaluating dislocation distributions associated with the deformation process from an already reported model [19], Eq. (10) of [3] was employed by using the heat evolved during stage 4, and all the pertinent quantities for Cu–3.4 at.% Sb required for this iterative solution. Calculations yielded a dislocation density ρ of approximately $8.5 \cdot 10^{14}$ m^{-2}.

Stage 2, associated with solute segregation to partial dislocation, allows determination of the temperatures suitable for performing isothermal calorimetry. Such temperatures, established in the previous section, are also shown in Fig. 1.

Dislocation character distribution

To verify that only one process is occurring during the kinetic course (segregation to dissociated edge or screw dislocations), it is worthwhile to compare the experimental heats evolved during isothermal segregation with those calculated from the previous model [19]. Figure 2 depicts isothermal traces at the indicated temperatures that lie inside the half-width temperature range of stage 2 in the thermoanalytical curve in Fig. 1, characterizing solute segregation to partial dislocations. The small knee at the beginning of the reaction should correspond to the rapid high-temperature formation of δ′.

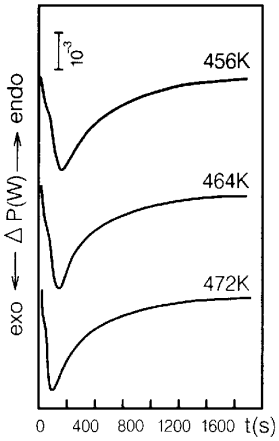

Fig. 2 Isothermal traces associated with the segregation process at the indicated temperatures

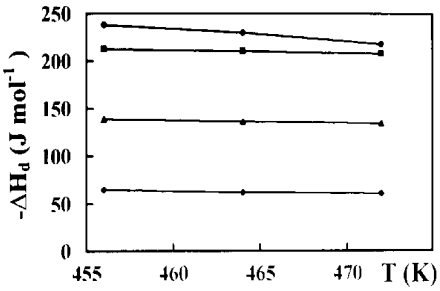

Fig. 3 Experimentally evolved heat ΔH_d (•) as a function of temperature, computed from the isothermal traces in Fig. 2. The calculated values of heats associated with different dislocation distributions are shown. ■– edge; ▲– half-edge – half-screw; ♦ – screw

Such experimental evolved heat values ΔH_d are shown in Fig. 3. It should be noted that, in spite of the narrow temperature range necessary, a small decrease in the equilibrium value of the evolved heat is observed, in accordance with the smaller equilibrium value of the concentration of pinned solute atoms expected as the temperature increases. Figure 3 also shows the evolved heats calculated from the recently developed model for each dislocation character distribution indicated [19]. This model predicts that in general an exothermic heat effect associated with the segregation of solute atoms to partial dislocation can be expressed as

$$\Delta H_d = 2\frac{\rho b^2}{c}\int_0^{\pi/2} f(\varphi)[\Delta H_{a1}(\varphi)c_{d1}(\varphi) + \Delta H_{a2}(\varphi)c_{d2}(\varphi)]d\varphi \tag{8}$$

ρ being the dislocation density, b the Burgers vector, c the alloy concentration, $f(\varphi)$ the probability density function of the dislocation character φ, $\Delta H_{a1}(\varphi)$ and $\Delta H_{a2}(\varphi)$ the maximum misfit interaction energies for the edge component of the leading and trailing dislocations with a solute atom, and $c_{d1}(\varphi)$ and $c_{d2}(\varphi)$ the equilibrium concentrations at the partials assumed here to follow Boltzmann statistics, i.e.

$$c_{d1,d2} = c\exp\frac{-\Delta H_{a1,a2}}{RT} \tag{9}$$

where subscripts 1 and 2 apply again to the leading and trailing dislocations, respectively, T is the equilibrium temperature and R is the gas constant.

When half-edge and half-screw dislocations are present, reference [20] showed that

$$\Delta H_d = \pi\frac{\rho}{c}b^2[\Delta H_{ae}c_{de} + \Delta H_{as}c_{ds}] \tag{10}$$

where ΔH_{ae} and ΔH_{ds} are the maximum binding energies, c_{de} and c_{ds} are the equilibrium concentrations of the solute at partials, and subscripts e and s refer to edge and screw dislocation character. If only dissociated edge dislocations are present

$$\Delta H_d = 2\pi \frac{\rho}{c} b^2 \Delta H_{ae} c_{de} \tag{11}$$

while if only screw dislocations are present

$$\Delta H_d = 2 \frac{\pi\rho}{c} b^2 \Delta H_{as} c_{ds} \tag{12}$$

The different values of ΔH_d were computed by taking c=0.034 and $\rho=8.5\cdot10^{14}$ m^{-2}, calculated from the recrystallization peak in Fig. 1. The corresponding ΔH_{ae} and ΔH_{as} values were computed from the general expression given by Eshelby [25] and Saxl [26] for the misfit interaction energy

$$\Delta H_a = \frac{1+\upsilon}{2\pi(1-\upsilon)} G b^3 \frac{b_e}{r} e_a \sin\theta \tag{13}$$

The maximum misfit interaction energy for the edge component of the leading dislocation with a solute atom occurs when $r=b$ and $\theta=-(\pi/2)$, r and θ being the coordinates at which the solute is located. The shear modulus G=44.2 GPa and the Poisson ratio υ=0.343 were taken from Hopkin *et al.* [27] and $e_a=d\ln a/dc$=0.2425 from the data of King [28]. For the edge component of a partial belonging to an extended edge dislocation, $b_e=0.5b$, and for an edge component of a partial belonging to an extended screw dislocation, $b_e=\sqrt{3}\,b/6$, where $b=\sqrt{2}\,a/2$ and $a=0.3644\cdot10^{-9}$ m [29] is the alloy lattice parameter. With the above quantities, $\Delta H_{ae}=-22.1$ kJ mol^{-1} and $\Delta H_{as}=-12.6$ kJ mol^{-1} are obtained. The values of ΔH_d for Eqs (10), (11) and (12) decrease slightly with temperature; this is shown in Fig. 3. It may be noticed that the model predicts that mostly edge dislocations develop during the experimental treatment of the alloy in the present research work. Hence, when studying the kinetics of solute segregation to partials corresponding to dissociated edge dislocations, only one process is expected, while mostly half-edge and half-screw dislocations are present in cold-rolled materials [19, 20]. Thus, any change in diffusion mechanism is likely to be detected during the segregation kinetic path because masking effects arising from overlapping segregation to both screw and edge dislocations are now minimized or completely eliminated.

Phenomenological approach to segregation kinetics

The actual mechanisms responsible for segregation during the annealing of Cu–3.4 at.% Sb with the previous deformation treatment may differ significantly from the formal treatment, hence, Q_f in Eq. (5) is replaced by Q_a, which is simply an 'apparent' activation energy of the process occurring here, K_f is replaced by K_a and n_b in K_o is replaced by a, so that Eq. (7) on generalization becomes

$$y = 1 - \exp(-K_a t^a) \tag{14}$$

with $K_a=A\exp(-Q_a/RT)$. Here, parameters A and a may not be constants. Then, substitution of this expression for K_a in Eq. (14) and rearrangement gives

$$\ln\ln(1-y)^{-1} = -\frac{Q_a}{RT} + a\ln(t) + \ln(A) \tag{15}$$

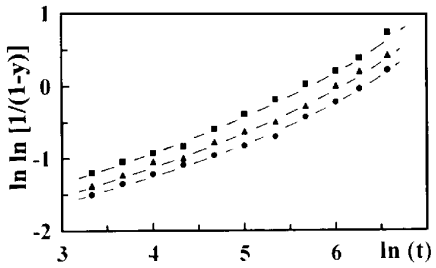

Fig. 4 $\ln\ln(1-y)^{-1}$ curves *vs.* $\ln(t)$

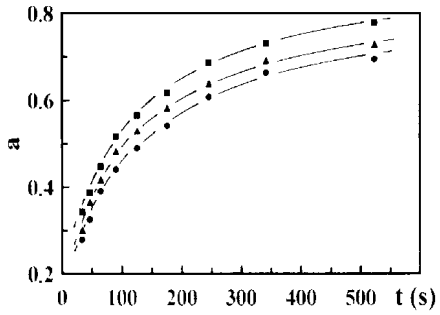

Fig. 5 Experimental time–temperature-dependent exponent *a vs.* time

A resolution empirical expression for the time–temperature dependent parameter a was obtained from the data after the testing of some probable analytical dependences, based on the fact that a increases slightly with increasing temperature and time. To simplify the analysis, this parameter, which is the slope of the curves in Fig. 4, was fitted to

$$a = c_1\ln(t) - \frac{c_2}{T} \tag{16}$$

where average values of c_1=0.14 and c_2=90.14 were obtained. This parameter is shown *vs.* time in Fig. 5. When Eq. (16) is inserted into Eq. (15), followed by rearrangement and simplification

$$\ln\ln(1-y)^{-1} = -\left[\frac{Q_a}{R} + c_2\ln(t)\right]\frac{1}{T} + \ln(A) + c_1[\ln(t)]^2 \tag{17}$$

which, for a fixed annealing time t, is in the form of $y=mx+b$. According to Eq. (17), the reacted fraction for the range of annealing temperatures and fixed annealing times will fall on a straight line in a ln–ln plot with a slope m equal to

$$m = -\left[\frac{Q_a}{R} + c_2 \ln(t)\right] \tag{18}$$

and an intercept

$$b = \ln(A) + c_1[\ln(t)]^2 \tag{19}$$

The apparent activation energy Q_a for the three annealing temperatures analysed was directly determined from Eq. (17) for different times. The slope of each straight line (determined by least-squares analysis) was used together with Eq. (18) to derive the apparent activation energy and is plotted in Fig. 6. It can be observed that Q_a increases with time, the increase appearing to be less steep as the reaction proceeds.

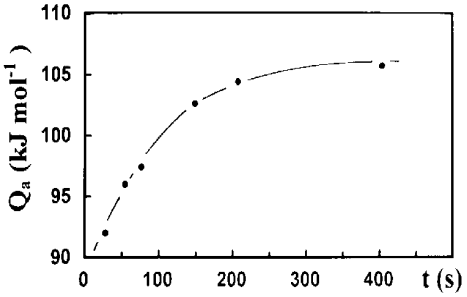

Fig. 6 Apparent activation energy Q_a *vs.* time

Discussion

Anneal hardening and the segregation process

Two main points should be considered during an analysis of the connection between anneal hardening and segregation.

Firstly, in the isothermal calorimetric experiments it was assumed that the dislocation density remains essentially the same during the run. This assumption is justified by the following arguments:

a) Recrystallization does not occur because the recrystallization temperature is shifted by the presence of solute atoms to 685 K, as detected in non-isothermal experiments (Fig. 1), as compared with the isothermal segregation temperatures at which the experiments were carried out, 456–472 K.

b) If it did occur, a large heat effect would overlap the segregation peak, which is not the case. Solute atoms also delay recrystallization [30]; this means that, under isothermal runs, for comparable initial conditions, annealing at a given temperature will require a longer time to achieve recrystallization.

c) As regards the recovery effects, these are likely to be negligible, because the low stacking fault energy of the alloy under study produces wide stacking faults during deformation, with the result that cross-slip is hindered and the slip distances are

consequently short. Moreover, in low stracking fault energy alloys, dislocation rearrangement processes via climb are extremely difficult, if not impossible [31].

d) If some recovery did take place, an associated heat effect would be detected in the isothermal trace, which was again not the case.

e) Segregation of solute to partial dislocations in turn inhibits itself; as revealed by the increased hardness values measured after segregation, dislocation motion during the annealing process is completed to equilibrium at temperature T, as shown in Fig. 7. The assumption that the dislocation density remains essentially constant during the annealing treatment is therefore justified in view of the above arguments.

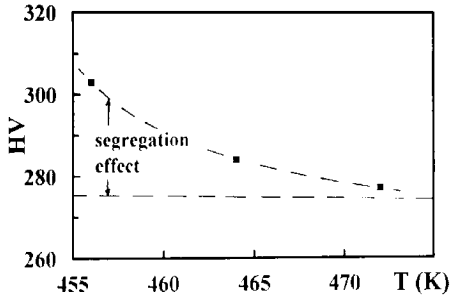

Fig. 7 Microhardness *vs.* annealing temperature after equilibrium is reached

Secondly, it is also expected that solute atoms should segregate to stacking faults, thereby changing the stacking fault energy and the distance between the partials. However, the alloy under study exhibits the largest stacking fault probabilities reported among the binary Cu alloys [22], and hence the distance between the partials should be several times the Burger's vector. Hence, the segregation process to one partial is hardly affected by the other partial, even if the stacking fault energy is changed to some extent by Suziki segregation. Consequently, if the heat of segregation to partials is somewhat affected, this should be considered a second-order effect. These arguments are considered at the beginning of the discussion. That segregation is responsible for a hardness increase is further confirmed if such values are confronted with the segregated fraction f_d of the solute to partial dislocations. In its general form, this fraction can be readily obtained from Eq. (8) as

$$f_d = 2\pi\rho b^2 \int_0^{\pi/2} f(\varphi)[\Delta H_{a1}(\varphi)c_{d1}(\varphi) + \Delta H_{a2}(\varphi)c_{d2}(\varphi)]d(\varphi) \tag{20}$$

which for the present case, where only extended edge dislocations are present, becomes

$$f_d = 2\pi\rho b^2 \exp\left(-\frac{\Delta H_{ae}}{RT}\right) \tag{21}$$

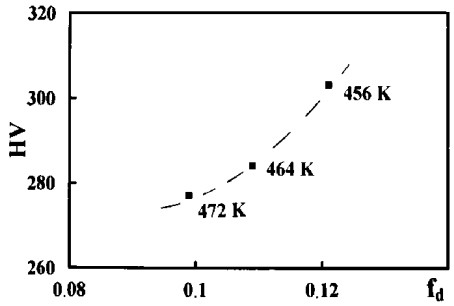

Fig. 8 Microhardness *vs.* segregated solute fraction f_d after equilibrium is reached at the indicated annealing temperatures

The *HV vs.* f_d values are shown in Fig. 8, and confirm unequivocally that the segregation phenomenon studied here is the main cause of anneal hardening.

The time-dependent apparent activation energy, Q_a

To analyse the experimental values of activation energy, it is necessary to consider that diffusion enhancement due to deformation is reflected by pipe diffusion along dislocations. Pipe diffusion may result because, after the deformation process, a gliding dislocation arrested by a less mobile forest dislocation will then increase its solute concentration mainly by the passage of solute from the more anchored forest to the less anchored gliding dislocation. Thus, the effective diffusion coefficient can be written as $D=D_p g+D_b(1-g)$, where D_p is the pipe diffusion coefficient, D_b is the lattice diffusion coefficient, and g is the atom fraction associated with the pipe. Assuming that the dislocation core cross-section contains 2 atoms, $g=2\Omega_o\rho/b_p$, in which Ω_o is the atomic volume, and $b_p=0.58\ b$ is Burger's vector of a partial dissociated edge or screw dislocation. Even for extremely high dislocation densities, $g<<1$, giving $D=D_p g+D_b$. At temperatures below half the melting point, most of the segregation takes place and $D_p g$ is much greater than D_b [32], thereby yielding $D\approx D_p g$ or $D=(2\Omega_o\rho/b_p)D_{op}\exp[-(Q_p/RT)]$, where the activation energy for pipe diffusion Q_p was taken similar to that of grain boundary diffusion [11], which in turn is a little more than half of that for volume diffusion; a value of $Q_b\approx 174.0$ kJ mol^{-1} was calculated from the Brown and Ashby correlations [33].

On the other hand, the pre-exponential factor of D_p can be taken from the lattice diffusion $D_{op}=D_{ob}$, which was calculated from [34, 35] as

$$D_{ob} = D_{oo}\left[kT_m(c)\frac{a_o^2(c)}{M(c)}\right]^{1/2} \tag{22}$$

Here, $D_{oo}=400$ for *fcc* structures [36], k is the Boltzman constant, $T_m(c)$ is a characteristic temperature equal to the mean line of the solidus and liquidus, $a(c)$ is the

lattice parameter of the alloy ($0.3644 \cdot 10^{-9}$ m) and $M(c)$ the mass 'average' AB atom given by the expression

$$\frac{1}{M(c)} = \frac{c}{M_{Sb}} + \frac{(1-c)}{M_{Cu}} \tag{23}$$

From the Cu–Sb equilibrium diagram, $T_m(c)$=1183 K was measured for 3.4 at.% Sb, while $M(c)=10.72 \cdot 10^{-26}$ kg at^{-1} was computed by taking $M_{Sb}=20.218 \cdot 10^{-26}$ kg at^{-1} and $M_{Cu}=10.55 \cdot 10^{-26}$ kg at^{-1}. With this procedure, a value of $D_{ob}=6.07 \cdot 10^{-5}$ m^2 s^{-1} was obtained.

On the other hand, for instance at 472 K, which is the highest temperature used in isothermal runs, taking $\Omega_o=7.48 \cdot 10^{-30}$ m^3, $b=2.58 \cdot 10^{-10}$ m [30] and the calculated value of $\rho=8.5 \cdot 10^{14}$ m^{-2} yields D/D_b amounting to about $5.8 \cdot 10^4$, strongly indicating that most of the diffusion occurs along dislocations, although the experimental values of Q_a are somewhat higher than Q_p=87.4 kJ mol^{-1} [31]. Thus, activation energy Q_a, which does not follow the formal treatment described hereafter, should be regarded as an apparent one that may be a weighted value between Q_p and Q_b according to

$$Q_a = \alpha(t)Q_p + [1 - \alpha(t)]Q_b \tag{24}$$

where α is a strengthening parameter that varies during the segregation reaction. As $Q_p \approx Q_b/2$; $Q_a=Q_b[1-\alpha/2]$. Then, by using Eq. (18):

$$\alpha(t) = 2\left[1 + \frac{R}{Q_b}(c_2 \ln(t) + m)\right] \tag{25}$$

which is a function of t only in the present approach.

As seen before, Q_a is closer to the values corresponding to pipe diffusion, although always increasing with time. In fact, if the binding energy is not negligible, as in the present case, then the solute can change the pipe structure, for example fill in open spaces and hinder atom movement along dislocations (pinner effects). This effect cannot be quantified simply, and there is no accepted theory on solute diffusion or on the effects of solutes on such diffusion, as there is for lattice diffusion. The above effect should increase the apparent activation energy, which depends on the

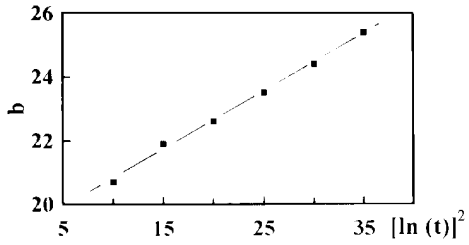

Fig. 9 Parameter b as a function of $[\ln (t)]^2$

magnitude of the binding energy. Therefore, as the occurrence of this mechanism becomes more difficult, the atom flux from the bulk with diffusion activation energy, Q_b contributes more and more to the segregation process. The limiting final value of the strengthening parameter $\alpha(t)$ is then determined by the time at which the equilibrium solute segregated is reached.

Parameter A is constant when b is plotted *vs.* $[\ln(t)]^2$, in accord with Eq. (19). This straight line is shown in Fig. 9, with intercept $A=1.78\cdot10^8\ s^{-1}$, resulting in $c_1=0.15$, in very good agreement with the previously calculated value $c_1=0.14$.

The experimental time–temperature-dependent exponent a

As stated above, the present study has found experimentally a time–temperature variable exponent a. Further, the formal treatment predicts that for bulk diffusion and short times $n_b=2/3$ can be derived [23]; an analogous argument applied to pipe diffusion yields $n_p=1/3$ [37]. The long time approximation for bulk and pipe diffusion including concentration gradients leads to $n=1/2$ [38]. The exponent 2/3 for bulk diffusion is a consequence of the fact that solute distant up to a range r may diffuse to the dislocation during time t. For times sufficiently the diffusion distance r increases as $r\propto(D_b t)^{1/3}$ (D_b=diffusion constant) [23]. In the event of free diffusion in the volume only, solutes inside a tube of a radius r enclosing the dislocation core can arrive at it within time t. The volume of the tube being proportional to r^2, the line concentration of solutes pinned increases in proportional to $t^{2/3}$. It follows that $n_b=2/3$. In the case of pipe diffusion, the diffusion path is restricted to a line. Therefore, not the whole volume of the enclosing tube proportional to $r^2\propto t^{2/3}$ is the possible source for the solute diffusion within time t; instead, only the whole number of forest lines up to a length $r\propto t^{1/3}$ ending at the dislocation provides diffusion. Such a mechanism results in $n_p=1/3$ [37]. Specific questions concerning n have recently been discussed [39–41]. The value $n=1/3$ has also been reported occasionally in the literature for Al alloys [42, 43]. For these alloys, only one segregation process is expected to take place in the kinetics of segregation [41, 43], because its high stacking fault energy avoids dislocations to dissociate. The varying experimental exponent a found here might be consistent with a mechanism starting with pipe diffusion, together with increasing bulk diffusion for later stages when the pipes tend to be exhausted, both mechanisms being affected by the already solute-pinned atoms.

The results concerning apparent activation energies are also consistent with those obtained for a and its increase with time. In the present work, the exponent parameter a varies between 0.25 and 0.75 from the early stage to the final stages of the reaction, which covers the theoretical range predicted for pipe and bulk diffusion (1/3 and 2/3, respectively). Hence, this parameter is in principle a weighted value of exponents n_p and n_b and can be written as

$$a = \beta(t,T)n_p + [1 - \beta(t,T)]n_b \tag{26}$$

where $\beta(t)$ is again a strengthening factor, so that $a=(2/3)–(1/3)\beta$. Compared with Eq. (16), this yields

$$\beta(t,T) = 3\left(\frac{2}{3} - c_1 \ln(t) + \frac{c_2}{T}\right) \tag{27}$$

showing the $\beta(t,T)$ dependence of t and T. It is worth recalling that, while β is a function of t and T, α is a function of t only.

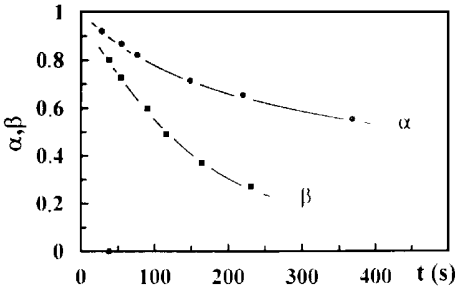

Fig. 10 Strengthening parameters α and β *vs.* time

As seen above, Q_a increases with time, but its values indicate that pipe diffusion prevails, while the time variation of a indicates a complete change from pipe to bulk diffusion. It is hard to decide which of these phenomenological kinetic parameters is more representative of the actual extent of change from pipe to bulk diffusion, but both reflect that this change actually exists in the frame of the approach used here. Figure 10 depicts the variation of the strengthening parameters α and β with time, with values of 1 for complete pipe diffusion, and 0 when only bulk diffusion exists. It may be noted that β decreases more rapidly than α in the course of the segregation reaction. No definitive conclusions can be drawn as concerns the reliability of the α and β values, since, as discussed in section dealing with the time dependent apparent activation energy, Q_a, pipe diffusion might be relatively more important than bulk diffusion throughout the whole segregation process, thereby favouring α reliability values, but β values were obtained on the basis of experimental data processing. Nevertheless, both parameters increase consistently as a function of time.

Finally, the observed increase in experimental exponent a with temperature might be consistent with the increased tendency to enhanced bulk diffusion in the segregation process when the temperature is raised. The temperature dependence of a was recently reported in connection with the kinetics of recovery [44] and crystallization [45]. At present, we are conducting work to establish theoretical support for its time–temperature dependence, empirically found both here and recently in Cu–3.34 at.% Sn [46].

Conclusions

This research leads to the conclusion that Cu–3.4 at.% Sb subjected to high plastic repeated deformation bending reveals, through a phenomenological approach, that the kinetics of solute segregation to the partial dislocations of dissociated edges is governed by two overlapping mechanism. Mostly diffusion along the pipes of the

partials occurs in a wide range during the reaction bulk solute diffusion, gradually becoming important. The excess of dissociated edge dislocations after the deformation treatment was confirmed by using a model previously developed by the authors.

* * *

The authors would like to thank the Fondo de Desarrollo Cientifico y Tecnológico (Fondecyt) for the financial support granted through Project 1980731, and the Instituto de Investigaciones y Ensayes de Materiales (Idiem), Facultad de Ciencias Físicas y Matemáticas, Universidad de Chile, for the facilities provided for this research.

References

1 R. W. Cahn and R. G. Davies, Phil. Mag., 5 (1960) 119.
2 J. M. Popplewell and J. Crane, Metall. Trans., 2 (1971) 3411.
3 A. Varschavsky, Mater. Sci. Eng., 89 (1987) 119.
4 A. Varschavsky, J. Mater. Sci., 26 (1991) 3603.
5 M. Z. Butt and Z. Rafi, J. Mater. Sci. Letts., 10 (1991) 309.
6 A. Varschavsky and E. Donoso, Mater. Sci. Eng., 32 (1978) 65.
7 E. Donoso and A. Varschavsky, Mater. Sci. Eng., 37 (1979) 151.
8 A. Varschavsky and E. Donoso, Mater. Sci. Eng., 40 (1979) 119.
9 S. S. Fan, K. Inai, S. Onaka and S. Miura, J. Soc. Mater. Sci. Jpn., 41 (1992) 607.
10 A. Varschavsky and E. Donoso, Res. Mechanica, 3 (1981) 195.
11 M. Militzer, W. P. Sun and J. J. Jonas, Acta Metall. Mater., 42 (1994) 133.
12 M. Z. Butt, Sci. Int., 2 (1990) 257.
13 F. R. N. Nabarro, Acta Metall., 9 (1990) 161.
14 A. Varschavsky, Scr. Metall., 9 (1975) 391.
15 L. P. Kubin, Y. Estrin and C. Perrier, Acta Metall. Mater., 40 (1992) 1037.
16 C. P. Ling, P. G. McCormick and Y. Estrin, Acta Metall. Mater., 41 (1993) 3323.
17 P. G. McCormick and P. Ling, Acta Metall. Mater., 43 (1995) 1969.
18 Y. Brechet and Y. Estrin, Acta Metall. Mater., 43 (1995) 955.
19 A. Varschavsky and E. Donoso, J. Thermal Anal., 48 (1997) 1229.
20 A. Varschavsky and E. Donoso, J. Thermal Anal., 50 (1997) 533.
21 A. Varschavsky and E. Donoso, Mater. Letts., 31 (1997) 239.
22 L. Deléhouzée and A. Deruyttere, Acta Metall., 15 (1967) 727.
23 A. H. Cottrell and B. A. Bilby, Proc. Roy. Soc. Lond., B62 (1949) 229.
24 N. Louat, Scripta Metall., 15 (1981) 1167.
25 J. D. Eshelby, In Physics of Metals, Defects. P. B. Hirsch, ed., Cambridge University Press, Vol. 2, 1975, p. 1.
26 I. Saxl, Czech J. Phys., 148 (1964) 381.
27 M. T. Hopkin, H. Pursey and M. F. Markham, Z. Metallk., 61 (1970) 535.
28 H. W. King, J. Mater. Sci., 1 (1966) 79.
29 W. B. Pearson, A Handbook of Lattice Spacing and Structures of Metals, Pergamon Press, London 1958, p. 597.
30 P. Cotterill and P. R. Mould, Recrystallization, Surrey University Press, 1976, p. 35.
31 Recrystallization of Metallic Materials. Ed. F. Haessner, Dr. Riederer Verlag, Stuttgart 1978, p. 137.
32 I. Dutte and D. L. Bourell, Acta Metall. Mater., 38 (1990) 2041.
33 A. M. Brown and M. S. Ashby, Acta Metall., 28 (1980) 1085.
34 A. Varschavsky and E. Donoso, J. Mater. Sci., 21 (1986) 3873.
35 D. L. Becke, I. Uzongi and F. J. Kedves, Phil. Mag. A, 44 (1981) 983.
36 D. L. Becke, G. Erdélyi and F. J. Kedves, J. Phys. Chem. Solids, 42 (1981) 163.

37 F. Springer and Ch. Schwink, Scripta Metall. Mater., 25 (1991) 2739.
38 F. R. Brotzen and A. Seeger, Acta Metall., 37 (1989) 2985.
39 J. Schlipf, Scripta Metall. Mater., 29 (1993) 287.
40 A. Kalk, A. Nortmann and Ch. Schwink, Phil. Mag. A, 72 (1995) 1239.
41 M. A. Morris, T. Lipe and D. G. Morris, Scripta Mater., 34 (1996) 1337.
42 C. P. Ling, P. G. McCormick and Y. Estrin, Acta Metall. Mater., 41 (1993) 3323.
43 P. G. McCormick and P. Ling, Acta Metall. Mater., 43 (1995) 1969.
44 J. Warren and A. D. Jackson, Scripta Mater., 34 (1996) 787.
45 M. P. Trujillo, A. Orozco, M. Casas-Ruiz, R. A. Ligero and R. Jiménez Garay, Mater. Letts., 24 (1995) 287.
46 A. Varschavsky and E. Donoso, Mater. Sci. Eng. (in press).